SCIENTIFIC OASIS

Spectrum of Mechanical Engineering and Operational Research

Journal homepage: www.smeor-journal.org
eISSN: 3042-0288

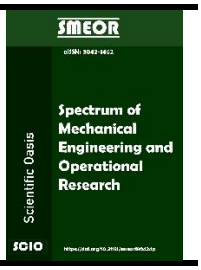

Nonclassical and Nonlinear Stability Analysis of Viscous Fluidic Piezoelectric Biomedical Nanosensor

Sayyid H. Hashemi Kachapi[1,*], Sayyideh Gh. Hashemi Kachabi [2]

[1] Department of Mechanical Engineering, Faculty of Engineering and Technology, University of Mazandaran, Babolsar, Islamic Republic of Iran
[2] Department of Physics, University of Kashan, Kashan, Islamic Republic of Iran

ARTICLE INFO

Article history:
Received 5 August 2024
Received in revised form 2 December 2024
Accepted 27 December 2024
Available online 29 December 2024

Keywords:
Piezoelectric biomedical nanosensor; Nonlinear frequency response; Stability; Critical fluid velocity; Gurtin–Murdoch surface/interface theory; Electrostatic and harmonic excitation.

ABSTRACT

In this paper, nonlinear vibration and stability analysis of viscous fluidic piezoelectric biomedical nanosensor (VFBNS) based on cylindrical nanoshell is investigated using the electro-elastic Gurtin–Murdoch surface/interface (S/I) theory. This piezoelectric nanoresonator is simultaneously subjected to visco-pasternak medium, electrostatic and harmonic excitations. The Hamilton's principle, the assumed mode method combined with Euler – Lagrange and also Complex averaging method combined with arc-length method are used to achieve the governing equations, boundary conditions and also the effect of different material, structural and excitations parameters on dimensionless natural frequency (DNF) (undamped $\bar{\Omega}_n$ and damped $\bar{\Omega}_d$), critical fluid velocity, nonlinear vibration and stability analysis of piezoelectric biomedical nanosensor. It is shown that the fluid velocity has major unpredictable effects on parametric studies of the system and one should precisely consider their effects. Also, it is concluded that ignoring the surface /interface effects leads to inaccurate results in vibrational response of the VFBNS. By changing the surface/interface parameters, the system stiffness is changed leading to nonlinear behavior of the system, which can be more or less pronounced compared to the case without the S/I effects accounted for. The obtained results of this study are useful for designing of nano/micro electro mechanical system and other nano-/micro-smart structures.

1. Introduction

In recent decades, the smart materials or adaptive structural systems, especially piezoelectric materials, have been widely used for application in numerous diverse fields of science and technology [1-5]. In these fields, nano structures, especially nano sensors/resonators, are widely used in modern engineering which have received considerable attention from researchers around the world, due to their unique features and widespread applications [6-10]. One of the most important scientific concepts in the design and fabrication of this nanosensor is the analysis of dynamic and vibrations considering nano-mechanical theories specially consideration of surface/interface effects. According

* *Corresponding author.*
E-mail address: shhashemi.kachapi@umz.ac.ir

https://doi.org/10.31181/smeor21202530

to the theory of Gurtin *et al.,* [11], surface/interface effects have vital role in their analysis and can affect the physical and chemical properties of nanomaterial. Investigation of the surface/interface elasticity on the mechanical behavior of nanostructures has become one of the attractive research areas in nanomechanics recently. Fang *et al.* [12] studied nonlinear vibration, buckling and postbuckling behavior of piezoelectric cylindrical nanoshells based on GM surface/interface theory. Zhu *et al.* [13] studied the size-dependent effect on the torsional buckling behavior of functionally graded cylindrical nano-shell covered with piezoelectric nano-layers based on the electro-elastic surface/interface theory. Ghorbanpour Arani *et al.* [14] studied nonlinear vibration of nano sheet conveying viscose fluid with small scale and surface effects. Surface stress effect on the vibration of nanoscale pipes based on a size-dependent Timoshenko beam model was investigated by Ansari *et al.* [15]. A new size-dependent nonlinear model for the analysis of the behavior of carbon nanotube resonators was introduced by Farokhi *et al.* [16] based on a modified couple stress theory. The numerical results are obtained for both static and dynamic cases, with special focus on the static pull-in behavior and on the effects of the newly developed electrostatic load model. The nonlinear vibration and the parametric oscillations of an electrostatically actuated piezoelectric nanobeam resonator were studied by Pourkiaee *et al.* [17] considering the surface elasticity theory. Sahmani *et al.* [18] used the Gurtin-Murdoch elasticity theory for the nonlinear buckling and postbuckling behaviors of nano-shell. Recently, Hashemi Kachapi *et al.* [19-22] presented semi-small scale approaches such as nonlocal, nonlocal strain gradient, Gurtin–Murdoch surface/interface theories and also combined different methods together to investigate the effects of the small scale on the natural frequencies, nonlinear vibration and stability analysis of single, double-walled and multi walled piezoelectric nano structures based on cylindrical nanoshell subjected to electrostatic and harmonic excitations.

In the present study, the nonlinear vibration and stability analysis of piezoelectric biomedical nanosensor conveying viscous fluid based on cylindrical nanoshell is investigated using the electro-elastic Gurtin–Murdoch surface/interface (S/I) theory. This piezoelectric nanoresonator is simultaneously subjected to visco-pasternak medium, electrostatic and harmonic excitations. The Hamilton's principle, the assumed mode method combined with Euler – Lagrange and Complex averaging method combined with arc-length method are used to obtain the governing equations, boundary conditions and also to investigate the effect of different material, structural and excitations parameters on dimensionless natural frequency (DNF), critical fluid velocity, nonlinear vibration and stability analysis of piezoelectric biomedical nanosensor.

2. Methodology

A piezoelectric biomedical nanosensor shown in Figure 1 consists of a cylindrical nanoshell with two piezoelectric layers embedded and a visco-Pasternak medium. The incoming bloodstream is considered as a viscous fluid with the fluid velocity u_f. The system is subjected to electrostatic force with direct electric voltage (V_{DC}) and harmonic excitation with amplitude f. In addition, this piezoelectric biomedical nanosensor, denoted as VFBNS, is actuated by the direct current polarization voltage V_p, which is applied along the thickness of the nanoshell. The length of the nanoshell is L, while the remaining geometric parameters of the cylindrical shell are: the mid-surface radius R, the thickness of cylindrical shell $2h_N$, and the thickness of piezoelectric material layer $2h_p$. With the origin of coordinate system located on the middle surface of nano-shell, the coordinates of a typical point in the axial, circumferential and radius directions are described by x, θ, and z, respectively. Also, K_w ,K_p and C_w are the stiffness coefficient of Winkler foundation, shear layer of Pasternak foundation and the damping factor of the visco medium for the transverse motion, respectively. The Young modulus, Poisson ratio and the mass density of cylindrical nano-shell are denoted by E_N, υ_N

and ρ_N, respectively. All of the physical and geometrical properties of the mentioned nanostructures for VFBNS can be seen in works done by Hashemi Kachapi *et al.,* [19-22].

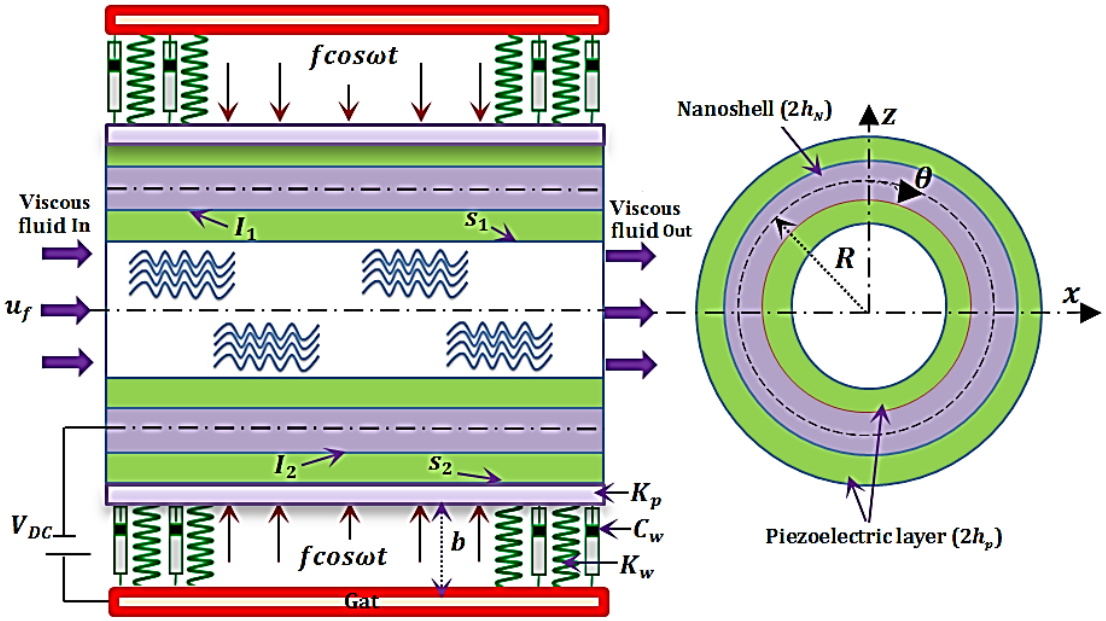

Fig. 1. Piezoelectric biomedical nanosensor (VFBNS) conveying viscous fluid

2.1 Non- classical Shell theory

Based on the Gurtin–Murdoch surface elasticity theory, the constitute relations for surfaces can be written as [11, 12]

$$\sigma_{\alpha\beta}^{s_k} = \tau_0^{s_k}\delta_{\alpha\beta} + \left(\tau_0^{s_k} + \lambda^{s_k}\right)\varepsilon_{qq}\delta_{\alpha\beta} + 2\left(\mu^{s_k} - \tau_0^{s_k}\right)\varepsilon_{\alpha\beta} + \tau_0^{s_k}u_{\alpha,\beta}^{s_k} - e_p^{s_k}E_{zp}, \quad (1)$$
$$\sigma_{\alpha z}^{s_k} = \tau_0^{s_k}u_{z,\alpha}^{s_k}, \qquad \sigma_{\alpha z}^{I_k} = \tau_0^{I_k}u_{z,\alpha}^{I_k}, (\alpha,\beta = x,\theta;\ \ k = 1,2)$$
$$\sigma_{\alpha\beta}^{I_k} = \tau_0^{I_k}\delta_{\alpha\beta} + \left(\tau_0^{I_k} + \lambda^{I_k}\right)\varepsilon_{qq}\delta_{\alpha\beta} + 2\left(\mu^{I_k} - \tau_0^{I_k}\right)\varepsilon_{\alpha\beta} + \tau_0^{I_k}u_{\alpha,\beta}^{s_1},$$

in which $\delta_{\alpha\beta}$ is the Kronecker delta function. Furthermore, the components of stress at the surfaces can be expressed as

$$\sigma_{xx}^{S_k} = (\lambda^{S_k} + 2\mu^{S_k})\varepsilon_{xx} + \left(\tau_0^{S_k} + \lambda^{S_k}\right)\varepsilon_{\theta\theta} - \frac{\tau_0^{S_k}}{2}\left(\frac{\partial w}{\partial x}\right)^2 + \tau_0^{S_k} - e_{31p}^{S_k}E_{zp}, \quad (2)$$
$$\sigma_{\theta\theta}^{S_k} = \left(\tau_0^{S_k} + \lambda^{S_k}\right)\varepsilon_{xx} + (\lambda^{S_k} + 2\mu^{S_k})\varepsilon_{\theta\theta} - \tau_0^{S_k}\left(\frac{w}{R} + \frac{1}{2R^2}\left(\frac{\partial w}{\partial\theta}\right)^2\right) + \tau_0^{S_k} - e_{32p}^{S_k}E_{zp},$$
$$\sigma_{xx}^{I_k} = (\lambda^{I_k} + 2\mu^{I_k})\varepsilon_{xx} + \left(\tau_0^{I_k} + \lambda^{I_k}\right)\varepsilon_{\theta\theta} - \frac{\tau_0^{I_k}}{2}\left(\frac{\partial w}{\partial x}\right)^2 + \tau_0^{I_k},$$
$$\sigma_{\theta\theta}^{I_k} = \left(\tau_0^{I_k} + \lambda^{I_k}\right)\varepsilon_{xx} + (\lambda^{I_k} + 2\mu^{I_k})\varepsilon_{\theta\theta} - \tau_0^{I_k}\left(\frac{w}{R} + \frac{1}{2R^2}\left(\frac{\partial w}{\partial\theta}\right)^2\right) + \tau_0^{I_k},$$
$$\sigma_{x\theta}^{(S,I)k} = \mu^{(S,I)k}\gamma_{x\theta} - \tau_0^{(S,I)k}\left(\frac{\partial v}{\partial x} + \frac{1}{R}\frac{\partial w}{\partial x}\frac{\partial w}{\partial\theta} - \frac{z}{R}\frac{\partial^2 w}{\partial x\partial\theta}\right), \sigma_{xz}^{(S,I)k} = \tau_0^{(S,I)k}\frac{\partial w}{\partial x},$$
$$\sigma_{\theta x}^{(S,I)k} = \mu^{(S,I)k}\gamma_{x\theta} - \tau_0^{(S,I)k}\left(\frac{1}{R}\frac{\partial u}{\partial\theta} + \frac{1}{R}\frac{\partial w}{\partial x}\frac{\partial w}{\partial\theta} - \frac{z}{R}\frac{\partial^2 w}{\partial x\partial\theta}\right), \sigma_{\theta z}^{(S,I)k} = \frac{\tau_0^{(s,I)k}}{R}\frac{\partial w}{\partial\theta},$$

Based on the classical continuum models, σ_{zz} is expressed as following:

$$\sigma_{zz} = \frac{1}{2}\left(\frac{\partial\left(\sigma_{xz}^{S_2} + \sigma_{xz}^{I_2}\right)}{\partial x} + \frac{1}{R}\frac{\partial\left(\sigma_{\theta z}^{S_2} + \sigma_{\theta z}^{I_2}\right)}{\partial \theta} - (\rho^{S_2} + \rho^{I_2})\frac{\partial^2 w}{\partial t^2}\right) \tag{3}$$
$$-\frac{1}{2}\left(\frac{\partial(\sigma_{xz}^{S_1} + \sigma_{xz}^{I_1})}{\partial x} + \frac{1}{R}\frac{\partial(\sigma_{\theta z}^{S_1} + \sigma_{\theta z}^{I_1})}{\partial \theta} - (\rho^{S_1} + \rho^{I_1})\frac{\partial^2 w}{\partial t^2}\right)$$
$$+\frac{z}{2h_N + 2h_p}\left(\frac{\partial\left(\sigma_{xz}^{S_2} + \sigma_{xz}^{I_2}\right)}{\partial x} + \frac{1}{R}\frac{\partial\left(\sigma_{\theta z}^{S_2} + \sigma_{\theta z}^{I_2}\right)}{\partial \theta} - (\rho^{S_2} + \rho^{I_2})\frac{\partial^2 w}{\partial t^2}\right)$$
$$+\frac{z}{2h_N + 2h_p}\left(\frac{\partial(\sigma_{xz}^{S_1} + \sigma_{xz}^{I_1})}{\partial x} + \frac{1}{R}\frac{\partial(\sigma_{\theta z}^{S_1} + \sigma_{\theta z}^{I_1})}{\partial \theta} - (\rho^{S_1} + \rho^{I_1})\frac{\partial^2 w}{\partial t^2}\right)$$

For simplification, the material properties of surfaces and interfaces are selected as

$$\tau_0^{S_1} = \tau_0^{S_2} = \tau_0^S,\ \lambda^{S_1} = \lambda^{S_2} = \lambda^S,\ \mu^{S_1} = \mu^{S_2} = \mu^S,\ e_{31p}^{S_1} = e_{31p}^{S_2} = e_{31p}^S,$$
$$\rho^{S_1} = \rho^{S_2} = \rho^S,\ e_{32p}^{S_1} = e_{32p}^{S_2} = e_{32p}^S, \tau_0^{I_1} = \tau_0^{I_2} = \tau_0^I,\ \lambda^{I_1} = \lambda^{I_2} = \lambda^I, \tag{4}$$
$$\mu^{I_1} = \mu^{I_2} = \mu^I, \rho^{I_1} = \rho^{I_2} = \rho^I,$$

According to Eq. (4), the normal stresses σ_{xx} and $\sigma_{\theta\theta}$ Eqs. (2) and (3) can be rewrite as

$$\sigma_{xx(N,p)} = C_{11(N,p)}\varepsilon_{xx} + C_{12(N,p)}\varepsilon_{\theta\theta} - e_{31p}\bar{E}_{xp} + \frac{\upsilon_{(N,p)}\sigma_{zz}}{1 - \upsilon_{(N,p)}}, \tag{5}$$

$$\sigma_{\theta\theta(N,p)} = C_{21(N,p)}\varepsilon_{xx} + C_{22(N,p)}\varepsilon_{\theta\theta} - e_{32p}\bar{E}_{\theta p} + \frac{\upsilon_{(N,p)}\sigma_{zz}}{1 - \upsilon_{(N,p)}}, \tag{6}$$

$$\sigma_{x\theta(N,p)} = C_{66(N,p)}\gamma_{x\theta}, \tag{7}$$

$$\sigma_{zz} = \frac{z}{h_N + h_p}\left((\tau_0^S + \tau_0^I)\left(\frac{\partial^2 w}{\partial x^2} + \frac{1}{R^2}\frac{\partial^2 w}{\partial \theta^2}\right) - (\rho^S + \rho^I)\frac{\partial^2 w}{\partial t^2}\right), \tag{8}$$

In the following formulations, all of the piezoelectric parameters (the materials and geometrical parameters) are neglected for the first layer and are, hence, assumed to be equal to zero, and all of the material and geometric parameters of nanoshell in the first layer are similar to the second layer of nanostructure. Also, all the coefficients and terms in Equations (5)–(8) such as nonlinear deflection, displacement fields and curvatures, relations of Gurtin–Murdoch surface/interface elasticity theory and etc. can be found in full detail in references [11, 12, 19–22].

3. Governing equations

In this section, at first the governing equations of motion of the piezoelectric cylindrical nanoshell are obtained by using the Hamilton's principle. The total strain energy considering the surface stress effect is expressed as:

$$\pi = \frac{1}{2}\int_0^L \int_0^{2\pi} \left\{ \begin{matrix} N_{xx}\varepsilon_{xx}^0 + N_{\theta\theta}\varepsilon_{\theta\theta}^0 + N_{x\theta}\gamma_{x\theta}^0 + \\ M_{xx}\kappa_{xx} + M_{\theta\theta}\kappa_{\theta\theta} + M_{x\theta}\kappa_{x\theta} + \eta_{33}\bar{E}_{zp}^2 h_p \end{matrix} \right\} R d\theta dx. \tag{9}$$

In Equation (9), the forces (N) and moment (M) resultants are defined in Hashemi Kachapi et al. [20-22] for FCBNS.

The kinetic energy of the FCBNS may be written as:

$$T = \frac{1}{2}\iint \left\{ I\left(\left(\frac{\partial u}{\partial t}\right)^2 + \left(\frac{\partial v}{\partial t}\right)^2 + \left(\frac{\partial w}{\partial t}\right)^2 \right) \right\} R d\theta dx \tag{10}$$

where

$$I = \int_{-h_N}^{h_N} \rho_N \, dz + \int_{-h_N-h_p}^{-h_N} \rho_p \, dz + \int_{h_N}^{h_N+h_p} \rho_p \, dz + \rho^{S,I} = 2\rho_N h_N + 2\rho_p h_p + 2\rho^S + 2\rho^I$$

Furthermore, the work done on the nano-shell by the viscoelastic medium, electrostatic force and the external harmonic excitation, respectively, can be expressed as [16, 23]

$$W_{vm} = -\int_0^L \int_0^{2\pi} \left\{ \int_0^w \left(K_w w - K_p \nabla^2 w + C_w \frac{\partial w}{\partial t} \right) dw \right\} R d\theta dx \tag{11}$$

$$W_e = \int_0^L \int_0^{2\pi} \left\{ \int_0^w \frac{\pi \Upsilon V_{DC}^2}{\sqrt{(b-w)(2R+b-w)} \left[\cosh^{-1}\left(1 + \frac{b-w}{R}\right) \right]^2} dw \right\} R d\theta dx \tag{12}$$

$$W_f = \int_0^L \int_0^{2\pi} \left\{ \int_0^w (f cos\omega t) dw \right\} R d\theta dx \tag{13}$$

where all the coefficients and terms appearing in Equations (11)– (13) can be found in references [20-22]. Also, the external work of the fluid can be expressed as [24]:

$$\begin{aligned} W_f &= \frac{1}{2}\int_0^L \int_0^{2\pi} F_{fluid}\, w \, R d\theta dx \\ &= \frac{1}{2}\int_0^L \int_0^{2\pi} \left\{ \begin{array}{l} -\rho_f A_f \left(\dfrac{\partial^2 w}{\partial t^2} + 2\big(VCF \times V_{no-slip}\big)\dfrac{\partial^2 w}{\partial x \partial t} + \big(VCF \times V_{no-slip}\big)^2 \dfrac{\partial^2 w}{\partial x^2} \right) \\ +\mu A_f \left(\dfrac{\partial^3 w}{\partial x^2 \partial t} + \dfrac{\partial^3 w}{R^2 \partial \theta^2 \partial t} + \big(VCF \times V_{no-slip}\big)\left(\dfrac{\partial^3 w}{\partial x^3} + \dfrac{\partial^3 w}{R^2 \partial x \partial \theta^2} \right) \right) \end{array} \right\} w \, R d\theta d \end{aligned} \tag{14}$$

The equations of motion and corresponding boundary conditions of the VFBNS can now be derived as follows:

$$\delta u: \quad \frac{\partial N_{xx}}{\partial x} + \frac{1}{R}\frac{\partial N_{x\theta}}{\partial \theta} = I\frac{\partial^2 u}{\partial t^2}, \tag{15}$$

$$\delta v: \quad \frac{\partial N_{x\theta}}{\partial x} + \frac{1}{R}\frac{\partial N_{\theta\theta}}{\partial \theta} = I\frac{\partial^2 v}{\partial t^2}, \tag{16}$$

$$\begin{aligned} &\delta w: \quad \frac{\partial^2 M_{xx}}{\partial x^2} + \frac{2}{R}\frac{\partial^2 M_{x\theta}}{\partial x \partial \theta} + \frac{1}{R^2}\frac{\partial^2 M_{\theta\theta}}{\partial \theta^2} - \frac{N_{\theta\theta}}{R} + N_{xx}\frac{\partial^2 w}{\partial x^2} + \frac{\partial N_{xx}}{\partial x}\frac{\partial w}{\partial x} + \frac{N_{\theta\theta}}{R^2}\frac{\partial^2 w}{\partial \theta^2} \\ &+ \frac{1}{R^2}\frac{\partial N_{\theta\theta}}{\partial \theta}\frac{\partial w}{\partial \theta} + \frac{2}{R}N_{x\theta}\frac{\partial^2 w}{\partial x \partial \theta} + \frac{1}{R}\frac{\partial N_{x\theta}}{\partial x}\frac{\partial w}{\partial \theta} + \frac{1}{R}\frac{\partial N_{x\theta}}{\partial \theta}\frac{\partial w}{\partial x} = I\frac{\partial^2 w}{\partial t^2} + C_w\frac{\partial w}{\partial t} + K_w w \\ &- K_p\nabla^2 w - \left[\begin{array}{l} -\rho_f A_f \left(\dfrac{\partial^2 w}{\partial t^2} + 2\big(VCF \times V_{no-slip}\big)\dfrac{\partial^2 w}{\partial x \partial t} + \big(VCF \times V_{no-slip}\big)^2 \dfrac{\partial^2 w}{\partial x^2} \right) \\ +\mu A_f \left(\dfrac{\partial^3 w}{\partial x^2 \partial t} + \dfrac{\partial^3 w}{R^2 \partial \theta^2 \partial t} + \big(VCF \times V_{no-slip}\big)\left(\dfrac{\partial^3 w}{\partial x^3} + \dfrac{\partial^3 w}{R^2 \partial \theta^2 \partial x} \right) \right) \end{array} \right] \\ &- \frac{\pi \Upsilon V_{DC}^2}{\sqrt{(b-w)(2R+b-w)} \left[\cosh^{-1}\left(1 + \frac{b-w}{R}\right) \right]^2} - f cos\omega t, \end{aligned} \tag{17}$$

And the boundary conditions are:

$$\delta u = 0 \quad or \quad N_{xx}n_x + \frac{1}{R}N_{x\theta}n_\theta = 0, \tag{18}$$

$$\delta v = 0 \quad or \quad N_{x\theta}n_x + \frac{1}{R}N_{\theta\theta}n_\theta = 0, \tag{19}$$

$$\delta w = 0 \quad or \quad \left(\frac{\partial M_{xx}}{\partial x} + \frac{1}{R}\frac{\partial M_{x\theta}}{\partial \theta} + N_{xx}\frac{\partial w}{\partial x} + \frac{N_{x\theta}}{R}\frac{\partial w}{\partial \theta}\right)n_x + \left(\frac{1}{R}\frac{\partial M_{x\theta}}{\partial x} + \frac{1}{R^2}\frac{\partial M_{\theta\theta}}{\partial \theta} + \frac{N_{x\theta}}{R}\frac{\partial w}{\partial x} + \frac{N_{\theta\theta}}{R^2}\frac{\partial w}{\partial \theta}\right)n_\theta = 0, \tag{20}$$

$$\frac{\partial w}{\partial x} = 0 \quad or \quad M_{xx}n_x + \frac{1}{R}M_{x\theta}n_\theta = 0, \tag{21}$$

$$\frac{\partial w}{\partial \theta} = 0 \quad or \quad \frac{1}{R}M_{x\theta}n_x + \frac{1}{R^2}M_{\theta\theta}n_\theta = 0, \tag{22}$$

Therefore, in this paper, the assumed mode method is used to obtain the equations of motion using Euler–Lagrange method. Using the strain and kinetic energies Eqs. (9) and (10) and also work done on the nano-shell from Eqs. (11-14), the following dimensionless parameters can be obtained.

$$\begin{aligned}
&\bar{u} = \frac{u}{h_N}, \bar{v} = \frac{v}{h_N}, \bar{w} = \frac{w}{h_N}, \xi = \frac{x}{L}, \bar{b} = \frac{b}{h_N}, \bar{A}_{ijN} = \frac{A_{ijN}}{A_{11N}}, \bar{B}_{ijN} = \frac{B_{ijN}}{A_{11N}h_N}, \bar{D}_{ijN} = \frac{D_{ijN}}{A_{11N}h_N^2},\\
&\bar{A}_{ijp} = \frac{A_{ijp}}{A_{11N}}, \bar{A}^*_{ij} = \frac{A^*_{ij}}{A_{11N}}, \bar{B}_{ijp} = \frac{B_{ijp}}{A_{11N}h_N}, \bar{B}^*_{ij} = \frac{B^*_{ij}}{A_{11N}h_N}, \bar{D}_{ijp} = \frac{D_{ijp}}{A_{11N}h_N^2}, \bar{D}^*_{ij} = \frac{D^*_{ij}}{A_{11N}h_N^2},\\
&\bar{F}^*_{11N} = \frac{F^*_{11N}}{A_{11N}h_N}, \bar{F}^*_{11p} = \frac{F^*_{11p}}{A_{11N}h_N}, \bar{E}^*_{11N} = \frac{E^*_{11N}}{A_{11N}h_N^2}, \bar{E}^*_{11p} = \frac{E^*_{11p}}{A_{11N}h_N^2}, \bar{J}^*_{11N} = \frac{J^*_{11N}}{\rho_N h_N^2},\\
&J^*_{11p} = \frac{J^*_{11p}}{\rho_N h_N^2}, \bar{G}^*_{11N} = \frac{G^*_{11N}}{\rho_N h_N^3}, G^*_{11p} = \frac{G^*_{11p}}{\rho_N h_N^3}, \bar{N}^*_{xp} = \frac{N^*_{xp}V_0}{A_{11N}}, \bar{N}^*_{\theta p} = \frac{N^*_{\theta p}V_0}{A_{11N}}, \bar{M}^*_{xp} = \frac{M^*_{xp}V_0}{A_{11N}h_N},\\
&\bar{M}^*_{\theta p} = \frac{M^*_{\theta p}V_0}{A_{11N}h_N}, \bar{\tau}^s_0 = \frac{\tau^s_0}{A_{11N}}, m_0 = \frac{L}{R}, m_1 = \frac{L}{h_N}, m_2 = \frac{h_N}{R} = \frac{1}{\bar{R}}, \bar{h}_p = \frac{h_p}{R}, m_3 = \frac{I}{2\rho_N h_N},\\
&m_4 = \frac{h_p}{h_N}, \tau = t\sqrt{\frac{A_{11N}}{2\rho_N h_N L^2}} = \Omega t, \bar{\Omega} = \frac{\omega}{\Omega}, \bar{K}_w = \frac{K_w L^2}{m_3 A_{11N}}, \bar{K}_p = \frac{K_p}{m_3 A_{11N}}, \bar{C}_w = \frac{C_w \Omega \mathrm{L}^2}{m_3 A_{11N}},\\
&\bar{\rho}_f = \frac{\rho_f}{m_3\rho_N}, \bar{u}_f = \left(VCF \times V_{no-slip}\right)\sqrt{\frac{2\rho_N h_N}{A_{11N}}}, \bar{\mu}_f = \frac{\mu_f}{m_3}\sqrt{\frac{2h_N}{\rho_N A_{11N}L^2}}, \bar{V}_{DC} = \frac{V_{DC}}{V_0},\\
&\bar{V}_p = \frac{V_p}{V_0}, \bar{F}_e = \frac{\pi m_1^2 V_0^2 \Upsilon}{m_3 A_{11N}}, \bar{F} = \frac{fL^2}{A_{11N}m_3{h_N}^2},
\end{aligned} \tag{23}$$

Here, V_0 is a reference voltage, set to 1 V throughout this study [16].

In the current study, the electrostatic force Equation (9) can be expressed as a polynomial form that is solved by nonlinear curve-fitting problem of lsqcurvefit function in Matlab Toolbox using least-squares. Therefore, the dimensionless electrostatic work can be written as follows [19-22]:

$$W_e = \int_0^L \int_0^{2\pi} \{\bar{F}_e(\bar{V}_{DC} + \bar{V}_{AC}\cos(\bar{\omega}\tau))^2(\bar{C}_1 + \bar{C}_2\bar{w} + \bar{C}_3\bar{w}^2 + \cdots + \bar{C}_n\bar{w}^{n-1})\bar{w}\}\, d\theta d\xi \tag{24}$$

where $\bar{C}_1 - \bar{C}_n$ are constants. In according to the mentioned statement and the results obtained in this field, the nonlinear term of electrostatic force is close to the exact solution for polynomial function with the order three and greater.

4. Solution procedure

In this section, by applying the assumed mode method, the in-plane, transverse and shear deformations can be expressed as general coordinates and mode shape functions that satisfy the geometric boundary conditions, as follows [25]

$$\begin{bmatrix} u(x,\theta,t) \\ v(x,\theta,t) \\ w(x,\theta,t) \end{bmatrix} = \sum_{m=1}^{M_1}\sum_{j=1}^{N} \begin{bmatrix} \left[u_{m,j,c}(\tau)\cos(j\theta) + u_{m,j,s}(\tau)\sin(j\theta)\right]\chi_{mj}(\xi) \\ \left[v_{m,j,c}(\tau)\sin(j\theta) + v_{m,j,s}(\tau)\cos(j\theta)\right]\phi_{mj}(\xi) \\ \left[w_{m,j,c}(\tau)\cos(j\theta) + w_{m,j,s}(\tau)\sin(j\theta)\right]\beta_{mj}(\xi) \end{bmatrix} + \sum_{m=1}^{M_2} \begin{bmatrix} u_{m,0}(\tau)\chi_{m0}(\xi) \\ v_{m,0}(\tau)\phi_{m0}(\xi) \\ w_{m,0}(\tau)\beta_{m0}(\xi) \end{bmatrix} = \sum_{(i,r,s)=1}^{M_2+M_1\times N} \begin{bmatrix} u_i(\tau)\chi_i(\xi)\vartheta_i(\theta) \\ v_r(\tau)\phi_r(\xi)\alpha_r(\theta) \\ w_s(\tau)\beta_s(\xi)\psi_s(\theta) \end{bmatrix}, \tag{25}$$

Using dimensionless strain and kinetic energies, Eqs. (9) and (10), and also dimensionless applied works, Eqs. (11-14), and applying Lagrange- Euler equations, the equation of motion is written to the following form:

$$[(M)_u^u]\{\ddot{\bar{u}}\} + [(K)_u^u]\{\bar{u}\} + [(K)_u^v]\{\bar{v}\} + [(K)_u^w]\{\bar{w}\} + [(NL)_u^w]\{\bar{w}^2\} = \left[\bar{F}_{up}\right], \tag{26}$$

$$[(M)_v^v]\{\ddot{\bar{v}}\} + [(K)_v^u]\{\bar{u}\} + [(K)_v^v]\{v\} + [(K)_v^w]\{\bar{w}\} + [(NL)_v^w]\{\bar{w}^2\} = \left[\bar{F}_{vp}\right], \tag{27}$$

$$\begin{aligned}[(M)_w^w]\{\ddot{\bar{w}}\} + [(c)_w^w]\{\dot{\bar{w}}\} + [(K)_w^u]\{\bar{u}\} + [(K)_w^v]\{\bar{v}\} + [(K)_w^w - \bar{F}_{e2}(K_e)_w^w]\{\bar{w}\} \\ + [(NL)_w^u]\{\bar{w}\bar{u}\} + [(NL)_w^v]\{\bar{w}\bar{v}\} + [(NL)_{w2}^w - \bar{F}_{e3}(NL_{2e})_w^w]\{\bar{w}^2\} \\ +[(NL)_{w3}^w - \bar{F}_{e4}(NL_{3e})_w^w]\{\bar{w}^3\} = [\bar{F}_{we}] + \left[\bar{F}_{wp}\right] + [\bar{F}cos\bar{\Omega}\tau],\end{aligned} \tag{28}$$

where $(M), (c)$ and (K) are the mass, damping and linear stiffness matrices. $(NL)_u^w, (NL)_v^w$, and $(NL)_{w2}^w$ are the second-order nonlinear stiffness matrices and $(NL)_{w3}^w$ is the third-order nonlinear stiffness matrix. Also, K_e, NL_{2e} and NL_{3e} are the linear stiffness, second and third order nonlinear stiffness matrices for electrostatic force expansion, respectively. Also, $\bar{F}_{up}$, $\bar{F}_{vp}$ and $\bar{F}_{wp}$ are the applied loads – piezoelectric voltage and surface stress. All coefficients of mass, stiffness, linear and nonlinear terms and applied loads of Eqs. (26) - (28) are presented by Hashemi Kachapi [20-22].

5. Results and Discussions

A verification study is presented in the work by Hashemi Kachapi et al. [19-22] with full details for single-walled (SW) and double-walled (DW) piezoelectric nanostructures. In this section, the effect of different material, structural and excitations parameters on dimensionless natural frequencies (DNF), critical fluid velocity, nonlinear vibration and stability analysis of piezoelectric biomedical nanosensor conveying viscous fluid (bloodstream) are investigated using surface/interface effects. In order to simplify the presentation, CC, SS, CS and CF represent clamped edges, simply supported edges, clamped-simply supported edges and clamped-free edges, respectively. Furthermore, for simplification of the surface effect, SE is represented. The surface and bulk material properties of Al nano-shell and the PZT piezoelectric layer are shown in Tables 1 and 2, respectively [12].

Table 1
Surface and bulk properties of Al [12]

$E_N(GPa)$	v_N	$\rho_N(kg/m^3)$	$\lambda^I(N/m)$	$\mu^I(N/m)$	$\tau_0^I(N/m)$	$\rho^I(kg/m^2)$
70	0.33	2700	3.786	1.95	0.9108	5.46×10^{-7}

Table 2
Surface and bulk properties of PZT-4 [12]

$C_{11p}(GPa)$	$C_{22p}(GPa)$	$C_{12p}(GPa)$	$C_{21p}(GPa)$	$C_{66p}(GPa)$	$E_p(GPa)$
139	139	77.8	77.8	30.5	95
v_p	$\rho_p(kg\ m^{-3})$	$\eta_{33p}(10^{-8}\ F/m)$	$\lambda^S(N/m)$	$\mu^S(N/m)$	$\tau_0^S(N/m)$
0.3	7500	8.91	4.488	2.774	0.6048
$e_{31p}(C/m^2)$	$e_{32p}(C/m^2)$	$e_{31p}^S(C/m)$	$e_{32p}^S(C/m)$	$\rho^S(kg/m^2)$	
-5.2	-5.2	-3×10^{-8}	-3×10^{-8}	5.61×10^{-6}	

The remaining geometric parameters for bulk and surface of VFBNS used in the following cases are shown in Table 3 [23].

Table 3
Material and geometric parameters

$R(m)$	L/R	h_N/R	h_p/R	b/R	$C_w(N.S/m)$
1×10^{-9}	10	0.01	0.005	0.1	1×10^{-5}
$K_w(N/m^3)$	$K_p(N/m)$	$V_p(V)$	V_0	$V_{DC}(V)$	$V_{AC}(V)$
8.9995035×10^{17}	2.071273	1×10^{-5}	1	3	2
$\mu_f(pa.s)$	$\rho_f(kg/m^3)$	$u_f(m/s)$	$F(N)$		
3×10^{-3}	1060	50	100		

Dimensionless natural frequencies (undamped $\overline{\Omega}_n$ and damped $\overline{\Omega}_d$) versus dimensionless fluid (bloodstream) velocity $\bar{u}_f$ are presented in Figures 2-8 with respect to different material, structural and excitations parameters for stability analysis and estimation of critical fluid velocity of a SS piezoelectric biomedical nanosensor with $\bar{V}_{DC} = 5$ and $\bar{F} = 1.5 \times 10^{-2}$. As shown in these figures, the frequency decreases as the flow velocity increases. In following, the nonlinear vibration and stability analysis of piezoelectric biomedical nanosensor using numerical method based on the arc-length method is investigated. In this section, the effect of fluid velocity $\bar{u}_f$, different boundary conditions, direct voltage $\bar{V}_{DC}$, excitation force $\bar{F}$ and piezoelectric voltage $\bar{V}_p$ will be discussed based on the frequency response of VFBNS.

The development of dimensionless frequency $\overline{\Omega}$ versus fluid velocity $\bar{u}_f$ of the piezoelectric biomedical nanosensor for different boundary conditions (SS, CC and CS) is shown in Figure 2. It can be seen that for all boundary conditions, the natural frequenciy decreases with the increasing fluid velocity. Also, due to the system softening in SS boundary condition and the low natural frequency, VFBNS is at a lower critical fluid velocity than it is the case with the other boundary conditions. The systems with the CS and CC boundary conditions have higher critical fluid velocity due to being softer. For the zero natural frequency, VFBNS becomes unstable and this physically implies that the VFBNS losses its stability due to the divergence via a pitchfork bifurcation.

The effect of length-to-small radius ratio (L/R) on the dimensionless natural frequency $\overline{\Omega}_n$ versus dimensionless fluid velocity $\bar{u}_f$ for SS piezoelectric biomedical nanosensor is illustrated in Figure 3. It is evident that the natural frequency decreases with increasing L/R and as a result, the critical fluid velocity of the VFBNS increases with the increasing L/R ratio. As can be seen, the critical fluid velocity corresponding to the lowest investigated value of $L/R = 3$ is smaller than for the remaining investigated values of this ratio. This physically implies that first the VFBNS in $L/R = 3$ losses its

stability due to the divergence via a pitchfork bifurcation. The reason is that a higher L/R ratio leads to decrease in the VFBNS stiffness, and cause a lower natural frequency of VFBNS.

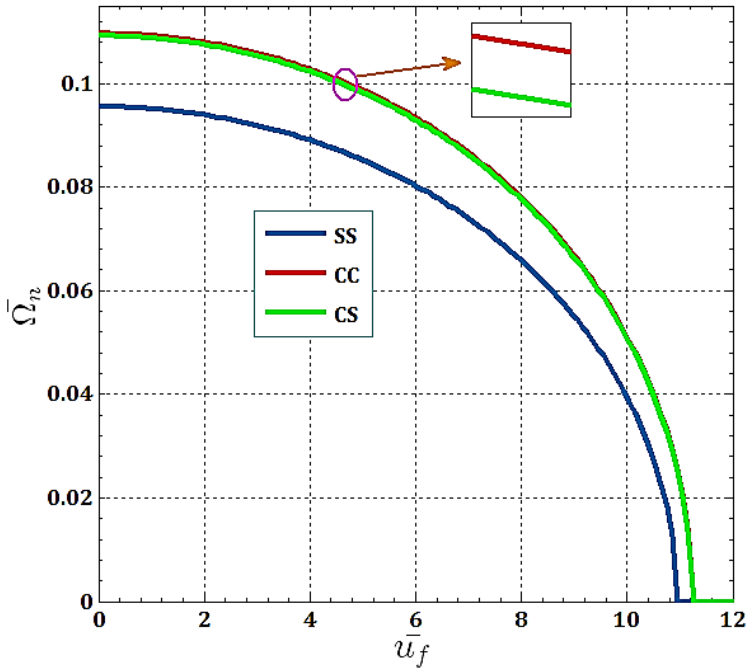

Fig. 2. The DNF ($\bar{\Omega}_n$) versus fluid velocity $\bar{u}_f$ of VFBNS for different boundary conditions

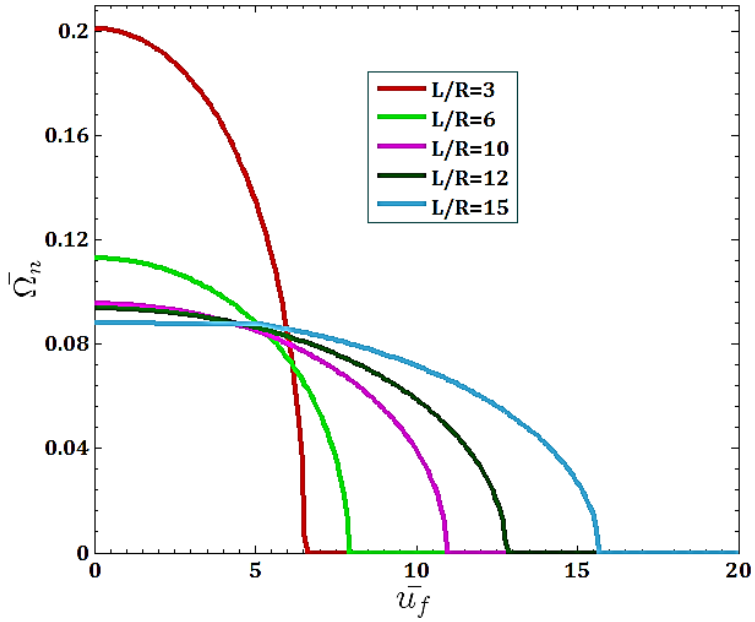

Fig. 3. The DNF ($\bar{\Omega}_n$) versus fluid velocity $\bar{u}_f$ of SS VFBNS for different values of L/R ratio

Figure 4 illustrates the effect of shell thickness to small radius ratio h_N/R on dimensionless natural frequencies $\bar{\Omega}_n$ versus dimensionless fluid velocity $\bar{u}_f$ for the SS piezoelectric biomedical nanosensor. It can be seen that with the increasing nanoshell stiffness ratio (h_N/R), the natural frequency $\bar{\Omega}_n$ and the critical fluid velocity $\bar{u}_f$ decrease. Also, the critical fluid velocity corresponding to the higher value of $h_N/R = 0.05$ is smaller than for the remaining investigated values of this ratio. This physically implies that first the VFBNS in $h_N/R = 0.05$ losses its stability due to the divergence via a pitchfork bifurcation.

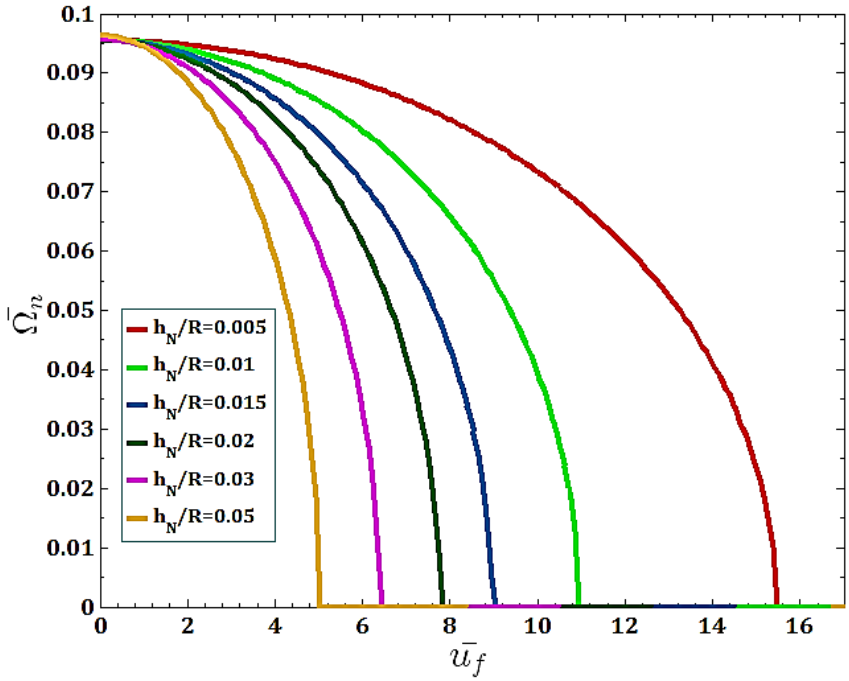

Fig. 4. The DNF versus fluid velocity $\bar{u}_f$ of SS VFBNS for different values of h_N/R ratio

The effect of piezoelectric thickness to small radius ratio (h_p/R) on dimensionless natural frequencies $\bar{\Omega}_n$ versus dimensionless fluid velocity $\bar{u}_f$ is presented in Figure 5. It can be seen that unlike the previous results for h_N/R ratio, in this case with the increasing h_p/R ratio, the DNF and the critical fluid velocity $\bar{u}_f$ increase. Also, the critical fluid velocity corresponding to the lower value of $h_p/R = 0.005$ is smaller than for the remaining investigated values of this ratio. This physically implies that first the VFBNS in $h_p/R = 0.005$ losses its stability due to the divergence via a pitchfork bifurcation.

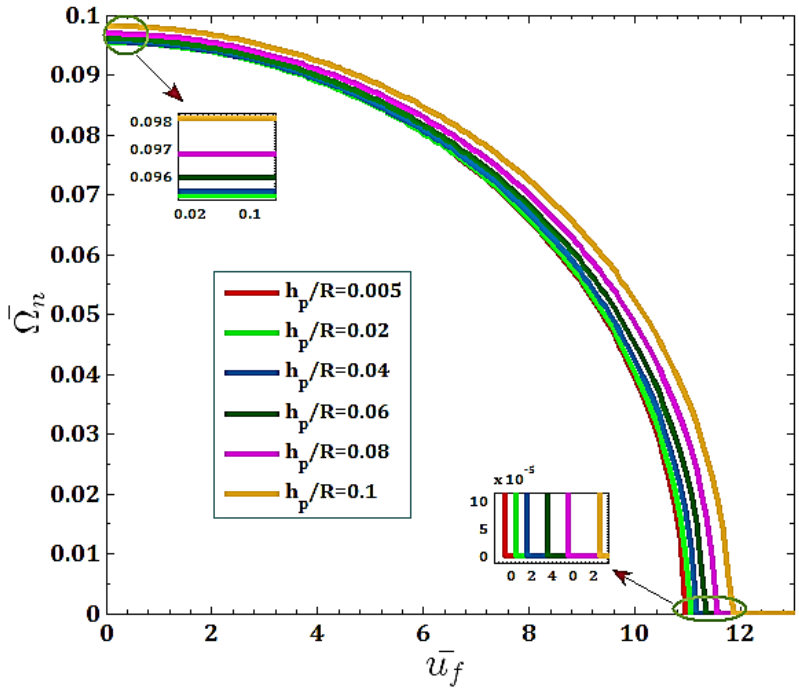

Fig. 5. The DNF ($\bar{\Omega}_n$) versus fluid velocity $\bar{u}_f$ of SS VFBNS for different values of h_p/R ratio

Figure 6 presents the effect of surrounding medium on dimensionless damped natural frequencies $\bar{\Omega}_d$ with respect to the dimensionless fluid velocity $\bar{u}_f$. As can be seen, five medium assumptions in this work are: with all visco-medium ($\bar{K}_w + \bar{K}_p + \bar{C}_w$), without visco-Winkler ($\bar{K}_w = \bar{C}_w = 0$), without visco-Pasternak ($\bar{K}_p = \bar{C}_w = 0$), without Winkler-Pasternak ($\bar{K}_w = \bar{K}_p = 0$) and without all visco-medium ($\bar{K}_w = \bar{K}_p = \bar{C}_w = 0$). It can be observed, when all visco-medium ($\bar{K}_w + \bar{K}_p + \bar{C}_w$) is considered, the critical velocity has the maximum values. In this case, the DNF also has the maximum value. This result indicates that the system is not very sensitive to the damping coefficient. Also, it is worth mentioning that DNF and critical velocity in Pasternak foundation are larger than DNF and critical velocity predicted by Winkler foundation. This is due to the fact that the Winkler foundation accounts for the effect of the normal stress of the elastic medium, whereas Pasternak elastic foundation accounts for the effect of the tangential and normal stresses of the elastic medium.

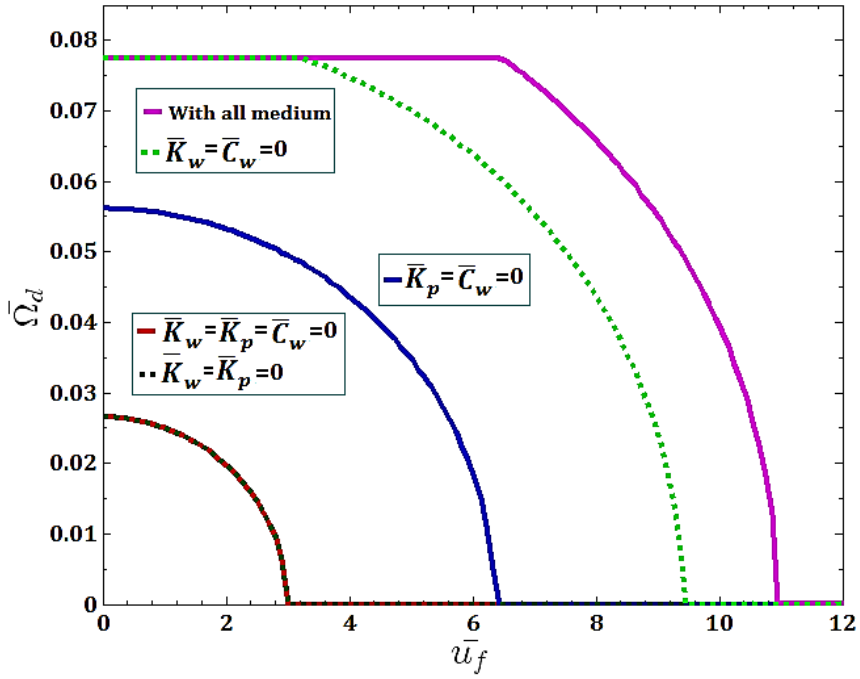

Fig. 6. The DNF ($\bar{\Omega}_n$) versus fluid velocity $\bar{u}_f$ of SS VFBNS for different cases of visco-medium

The effect of piezoelectric voltage $\bar{V}_p$ on dimensionless natural frequencies $\bar{\Omega}_n$ versus dimensionless fluid velocity $\bar{u}_f$ for SS piezoelectric biomedical nanosensor is illustrated in Figure 7. As shown in this figure, with the increasing $\bar{V}_p$, the natural frequency $\bar{\Omega}_n$ and the critical fluid velocity $\bar{u}_f$ also increase. This is presumably because the increasing piezoelectric voltage increases the nanoshell stiffness. Also, the critical fluid velocity corresponding to the lower value of $\bar{V}_p = 0$ is smaller than for the remaining investigated values of this ratio. This physically implies that first the VFBNS in $\bar{V}_p = 0$ losses its stability due to the divergence via a pitchfork bifurcation.

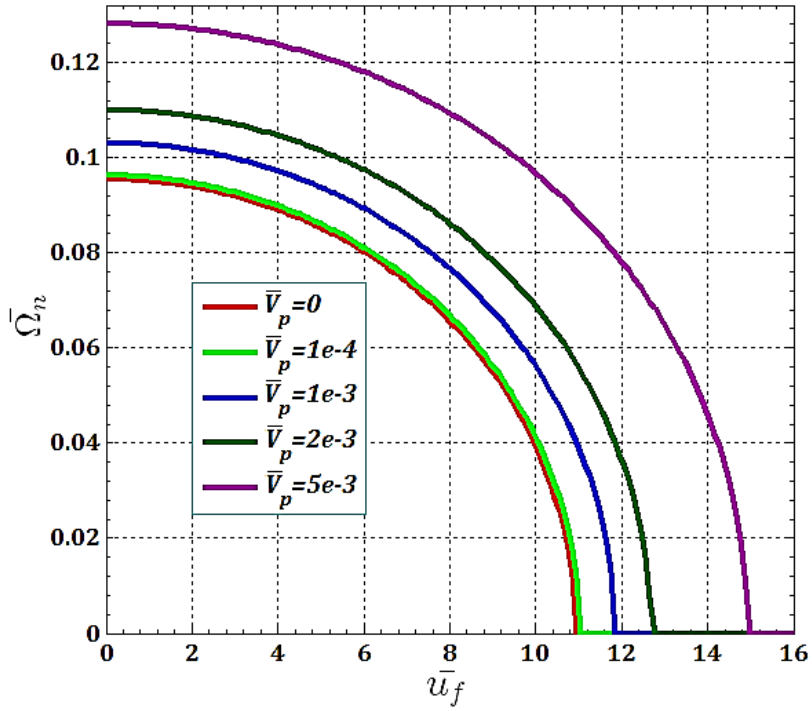

Fig. 7. The DNF ($\bar{\Omega}_n$) versus fluid velocity $\bar{u}_f$ of SS VFBNS for different values of $\bar{V}_p$

Dimensionless natural frequencies $\bar{\Omega}_n$ versus dimensionless fluid velocity $\bar{u}_f$ for SS piezoelectric biomedical nanosensor with and without surface/interface energy effects are shown in Figure 8.

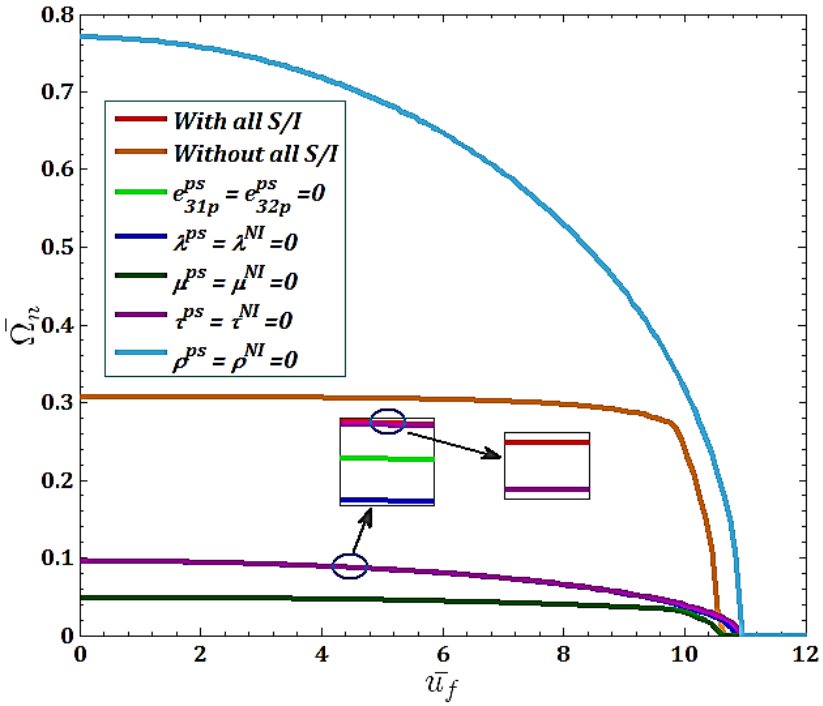

Fig. 8. Surface/interface energy effects on the DNF ($\bar{\Omega}_n$) versus fluid velocity $\bar{u}_f$ of SS VFBNS

It is obvious that the most important parameters influencing the natural frequencies and fluid velocity are surface/interface density (ρ^{ps}, ρ^{NI}). Regardless of these parameters (or for lower values of the parameters), due to the higher stiffness of VFBNS, the critical fluid velocity is higher than for

the remaining parameters and the system losses its stability due to the divergence via a pitchfork bifurcation, but the system also has the maximum natural frequency in this case. Also, in the case without the S/I effects, VFBNS has greater DNF than in the case with the S/I effects and smaller than in the case without surface/interface density. From this result it can be concluded that by changing the surface/interface densities, and thus increasing or decreasing the system stiffness, the resulting DNF can be lower or greater compared to the model that neglects the S/I effects. Also, in all cases, with increasing $\bar{u}_f$, the natural frequency decreases.

The effect of dimensionless fluid velocity $\bar{u}_f$ on nonlinear frequency response of SS piezoelectric biomedical nanosensor with $\bar{V}_{DC} = 5$ and $\bar{F} = 1.5 \times 10^{-2}$ is illustrated in Figure 9. The results show that with the increasing fluid velocity $\bar{u}_f$, due to the decreasing VFBNS stiffness, the resonance frequency $\bar{\Omega}$ decreases and the oscillation amplitude increases. The system displays softening-type nonlinear behavior with two saddle-node bifurcations.

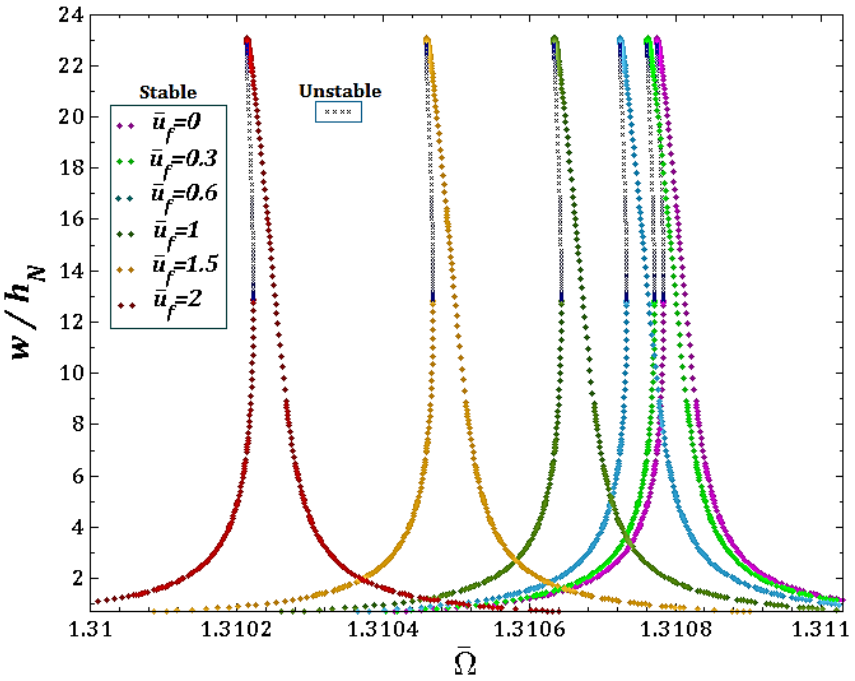

Fig. 9. The effect of fluid velocity $\bar{u}_f$ on nonlinear frequency response of SS VFBNS

The nonlinear frequency responses and stability analysis of the VFBNS with $\bar{V}_{DC} = 5$, $\bar{F} = 1.5 \times 10^{-2}$ and $\bar{u}_f = 1$ is presented in Figure 10 for different boundary conditions (SS, CC, CS and CF) and with all surface/interface effects accounted for. It can be seen that the CC boundary condition has the highest resonance frequency and the SS boundary condition has the highest resonance amplitude. In both cases (CC and CS), the amplitude of the resonance frequency and the type of system behavior (softening) as well as the range of instability are approximately the same and they are not much sensitive to the boundary conditions. Also, CF boundary condition is stable in all resonance frequencies and has a smaller resonance frequency and the amplitude compared to other boundary conditions.

In Figure 11, the effect of different direct electric voltage $\bar{V}_{DC}$ on the nonlinear frequency response and stability analysis of SS VFBNS is shown. The results show that with the increasing $\bar{V}_{DC}$ voltage, the oscillation amplitude also increases. Moreover, due to the increasing amplitude of the DC voltage (and, hence, the increasing amplitude of the static deflection), the system displays softening-type nonlinear behavior with two saddle-node bifurcations.

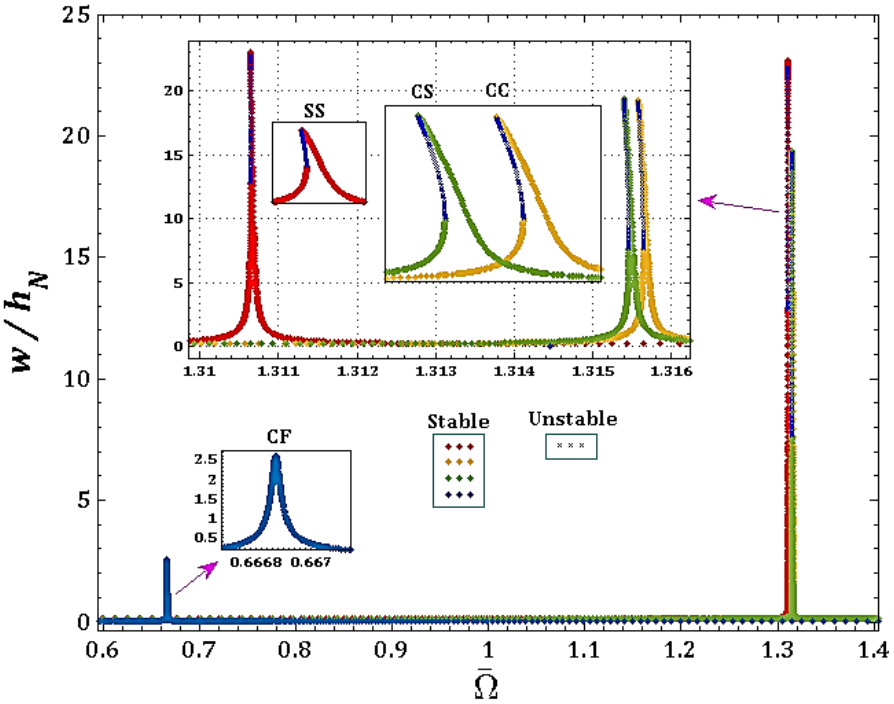

Fig. 10. The effect of different boundary conditions on the nonlinear frequency response and stability analysis of the SS VFBNS

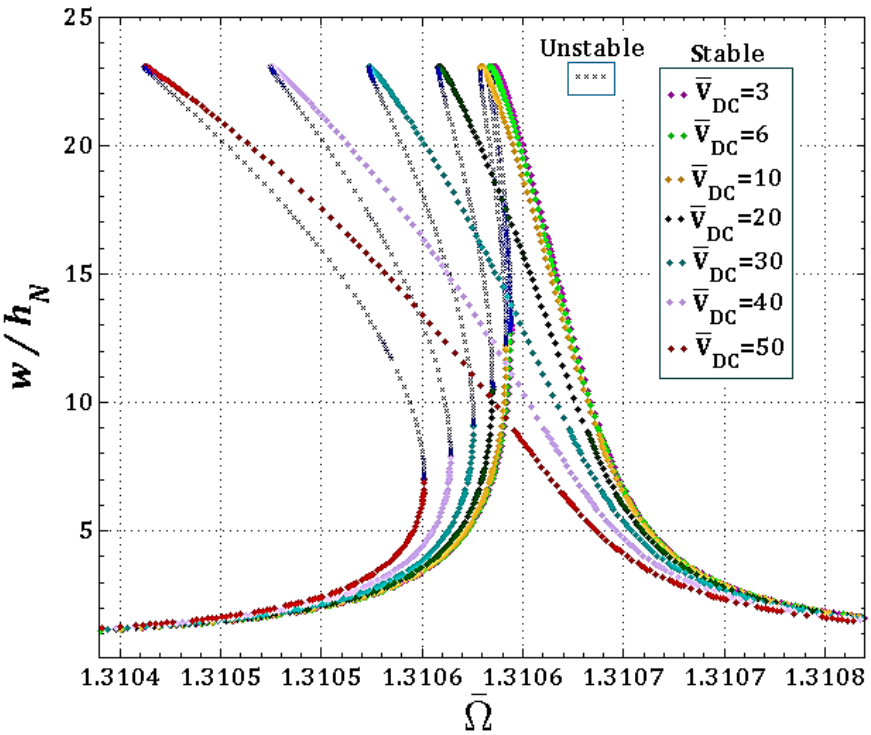

Fig. 11. The effect of direct voltage $\bar{V}_{DC}$ on nonlinear frequency response and stability analysis of SS VFBNS

The effect of the excitation force $\bar{F}$ on the nonlinear frequency response and stability analysis of SS VFBNS with $\bar{V}_{DC} = 20$ and $\bar{u}_f = 1$ is presented in Figure 12. The results show that with the increasing dimensionless excitation $\bar{F}$, the amplitude and the range of the VFBNS system's instability also increase with saddle-node bifurcations. Also, with the increasing range of instability and nano shell stiffness, the nonlinear softening behavior becomes more proncounced+.

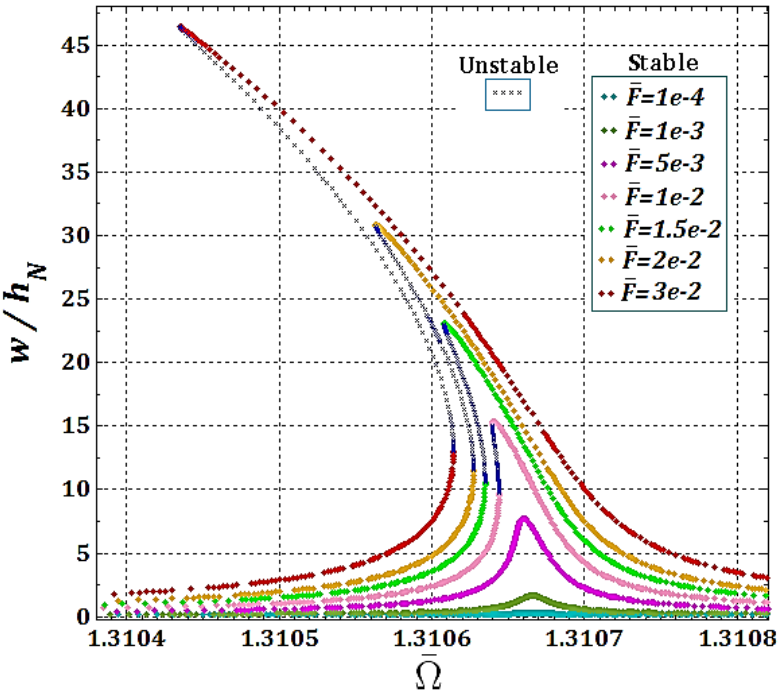

Fig. 12. The effect of excitation force $\bar{F}$ on the nonlinear frequency response and stability analysis of SS VFBNS

The effect of electrostatic excitation ($\bar{V}_{DC}$) and harmonic excitation ($\bar{F}$) on the nonlinear softening and hardening behavior of SS VFBNS is presented in Figure 13. The results show that, with the electrostatic force accounted for, the system is softened and moved to the left, while, if only the harmonic excitation is accounted fort, the softness of the SS VFBNS is reduced and tends to move to the right, implying that it exhibits hardening behavior. So, we conclude that the electrostatic force, which is a consequence of voltage DC, is the cause of nonlinear softening behavior of SS VFBNS.

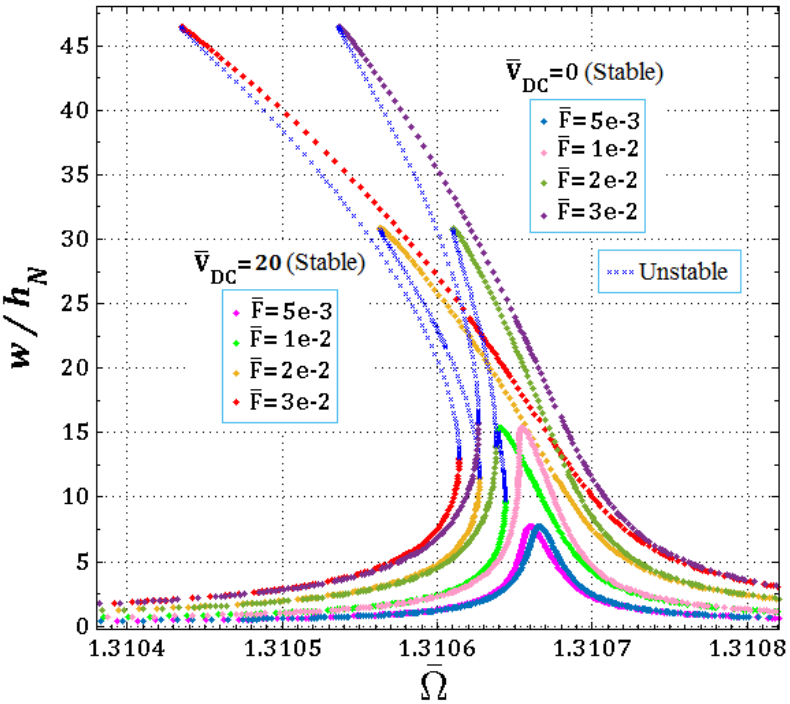

Fig. 13. The effect of electrostatic ($\bar{V}_{DC}$) and harmonic excitation ($\bar{F}$) on the nonlinear softening and hardening behavior of SS VFBNS

Finally, Figure 14 presents the effect of the piezoelectric voltage $\bar{V}_p$ with $\bar{V}_{DC} = 20, \bar{F} = 1.5 \times 10^{-2}$ and $\bar{u}_f = 1$ on the nonlinear frequency response and stability analysis of SS VFBNS. It can be seen that, as the piezoelectric voltage $\bar{V}_p$ increases, the resonance frequencies, static deformation and the oscillation amplitude of the VFBNS also increase and the instability occurs with a saddle-node bifurcation type accompanied by nonlinear softening-type behavior. Also, it is clear from the results that the piezoelectric voltage influences the resonant frequency and static deformation but has no significant effect on the nonlinear behavior and bandwidth.

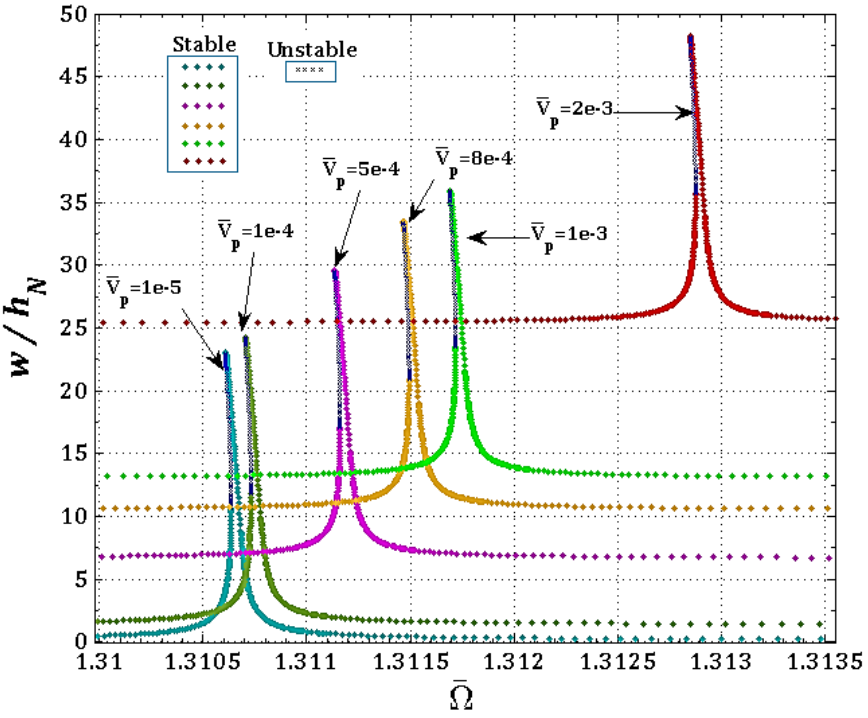

Fig. 14. The effect of piezoelectric voltage $\bar{V}_p$ on frequency response of SS VFBNS

6. Conclusion

In the current study, nonlinear vibration and stability analysis of piezoelectric biomedical nanosensor (VFBNS) conveying viscous fluid based on cylindrical nanoshell is investigated using the Gurtin–Murdoch surface/interface theory. This piezoelectric nanoresonator is simultaneously subjected to visco-pasternak medium, electrostatic and harmonic excitations. For this purpose, the Hamilton's principle, the assumed mode method combined with Euler – Lagrange and also Complex averaging method combined with arc-length method are used to derive the governing equations, boundary conditions and also to investigate the effect of different material, structural and excitations parameters on dimensionless natural frequency, critical fluid velocity, nonlinear vibration and stability of piezoelectric biomedical nanosensor.

The following conclusions are deduced from this study:

- In all boundary conditions, natural frequencies decrease with the increasing fluid velocity. Also, due to the system softening in SS boundary condition and low natural frequency, VFBNS is at a lower critical fluid velocity than for other boundary conditions. Upon the SS boundary condition, the CS and CC boundary conditions, respectively, reach the zero or critical fluid velocity.
- For zero natural frequency, VFBNS becomes unstable and this physically implies that the VFBNS loses its stability due to the divergence via a pitchfork bifurcation.

- Natural frequencies decrease with increasing L/R and as a result, the critical fluid velocity of the VFBNS increases. The reason is that a higher L/R ratio leads to decrease in the VFBNS stiffness, and, thus, cause lower natural frequencies of VFBNS.
- With the increasing nanoshell stiffness ratio (h_N/R), the natural frequency $\overline{\Omega}_n$ and the critical fluid velocity $\overline{u}_f$ decrease.
- With the increasing h_p/R ratio, the DNF and the critical fluid velocity $\overline{u}_f$ increase.
- When all visco-medium is considered, the critical velocity has the maximum values. In this case, the DNF also has the maximum value. This result indicates that, in all the considered cases, the system is not very sensitive to the damping coefficient.
- DNF and critical velocity in Pasternak foundation are larger than DNF and critical velocity predicted by Winkler foundation. This is due to the fact that the Winkler foundation accounts for the effect of the normal stress of the elastic medium, whereas Pasternak elastic foundation accounts for the effect of the tangential and normal stresses of the elastic medium.
- With increasing $\overline{V}_p$, the natural frequency $\overline{\Omega}_n$ and the critical fluid velocity $\overline{u}_f$ also increase. This is presumably because the increasing piezoelectric voltage increases the nanoshell stiffness.
- The most important parameters influencing natural frequencies and fluid velocity are the surface/interface density (ρ^{ps}, ρ^{NI}). Regardless of these parameters, due to higher stiffness of VFBNS, the critical fluid velocity reaches zero value faster than when compared to the system accounting for the remaining parameters. The system loses its stability, but has the maximum natural frequency in this case.
- In the case without the S/I effects accounted for, VFBNS has DNF greater than the case with S/I effects and smaller than the case without surface/interface density.
- By changing the surface/interface densities, and thus increasing or decreasing the system stiffness, the DNF can be lower or greater compared to the system not accounting the S/I effects.
- With increasing fluid velocity $\overline{u}_f$, due to decreasing VFBNS stiffness, the resonance frequency $\overline{\Omega}$ decreases and the oscillation amplitude increases.
- The CC boundary condition has the highest resonance frequency and the SS boundary condition has the highest resonance amplitude. In both cases (CC and CS), the amplitude of the resonance frequency and the type of system behavior (softening) as well as the range of instability are approximately the same. The CF boundary condition is stable in all resonance frequencies and has the minimum resonance frequency and amplitude compared to the other boundary conditions.
- With increasing $\overline{V}_{DC}$ voltage, the oscillation amplitude increases. Moreover, due to increasing amplitude of the DC voltage, the system displays softening-type nonlinear behavior with two saddle-node bifurcations.
- With increasing dimensionless excitation $\overline{F}$, the amplitude and the range of the VFBNS system's instability increase with saddle-node bifurcations.
- If the electrostatic force is accounted for, the system is softened and moved to the left, while if only the harmonic excitation is accounted for, the softness of the SS VFBNS is reduced and, hence it tends to move to the right and exhibits hardening behavior. So, we conclude that the electrostatic force duo to the voltage DC is the cause of nonlinear softening behavior of SS VFBNS.
- As piezoelectric voltage $\overline{V}_p$ increases, the resonance frequencies, static deformation and the oscillation amplitude of the VFBNS increase and instability occurs with saddle-node bifurcation type and nonlinear softening-type behavior.

Author Contributions
Conceptualization, Methodology, Software, Writing, S.H.H.K.; Supervision, Writing - Review & Editing, Validation, Project administration, S.G.H.K. All authors have read and agreed to the published version of the manuscript.

Funding
This research received no external funding.

Data Availability Statement
Not applicable.

Conflict of interest
The authors report no conflict of interest.

Funding Acknowledgement
This research received no specific grant from any funding agency in the public, commercial, or not-for-profit sectors.

References
[1] Rama, G., Marinkovic, D.Z., & Zehn, M.W. (2017). Linear shell elements for active piezoelectric laminates. *Smart Structures and Systems*, 20(6), 729-737. https://doi.org/10.12989/sss.2017.20.6.729.
[2] Duan, W.H., Wang, Q., & Quek, S.T. (2010). Applications of Piezoelectric Materials in Structural Health Monitoring and Repair: Selected Research Examples. *Materials*, 3, 5169-5194. https://doi.org/10.3390/ma3125169.
[3] Ganji, D. D., & Hashemi Kachapi, Sayyid Habibollah (2015). Application of Nonlinear Systems in Nanomechanics and Nanofluids: Analytical Methods and Applications (Micro and Nano Technologies), New York: Elsevier.
[4] Madunuri, C. S., Veena, E., Nagasamudram, S. K., Kadiyala, C. B. N., Mallikarjuna, A., & Basha, B. (2022). A Review on Piezoelectric Materials and Their Applications. *Crystal Research and Technology*, 58(2), 2200130. https://doi.org/10.1002/crat.202200130.
[5] Milić, P., Marinković, D., Klinge, S., & Ćojbašić, Ž. (2023). Reissner-Mindlin Based Isogeometric Finite Element Formulation for Piezoelectric Active Laminated Shells. *Tehnicki Vjesnik*, 30(2), 416 - 425. https://doi.org/10.17559/TV-20230128000280.
[6] Mousavi, S.M., Hashemi, S.A., Zarei, M., Amani, A.M., & Babapoor, A. (2018). Nanosensors for Chemical and Biological and Medical Applications. *Medicinal Chemistry,* 8, 205-217. https://doi.org/10.4172/2161-0444.1000515.
[7] Hashemi Kachapi, S.H., Dardel, M., Mohamadi daniali, H., & Fathi, A. (2019). Pull-in instability and nonlinear vibration analysis of electrostatically piezoelectric nanoresonator with surface/interface effects. *Thin-Walled Structures*, 143, 106210. https://doi.org/10.1016/j.tws.2019.106210.
[8] Mosayebi, R., Ahmadzadeh, A., Wicke, W., Jamali, V., Schober, R., & Nasiri-Kenari, M. (2018). Early Cancer Detection in Blood Vessels Using Mobile Nanosensors. arXiv 1805.08777. https://doi.org/10.48550/arXiv.1805.08777.
[9] Chatterjee, K., Sarkar, S., Rao, K. J., & Paria, S. (2014). Core/shell nanoparticles in biomedical applications. *Advances in Colloid and Interface Science*, 209, 8–39. https://doi.org/10.1016/j.cis.2013.12.008.
[10] Choi, Y.E., Kwak, J.W., Park, J.W. (2010). Nanotechnology for Early Cancer Detection. *Sensors*, 10(1), 428-455. https://doi.org/10.3390/s100100428.
[11] Gurtin, M.E., & Murdoch, A.I. (1978). Surface stress in solids. *International Journal of Solids and Structures,* 14,431–440. https://doi.org/10.1016/0020-7683(78)90008-2.
[12] Fang, X.Q., Zhu, C.S., Liu, J.X., & Zhao, J. (2018). Surface energy effect on nonlinear buckling and postbuckling behavior of functionally graded piezoelectric cylindrical nanoshells under lateral pressure. *Materials Research Express,* 5(4), 045017. https://doi.org/10.1088/2053-1591/aab914.
[13] Zhu, C.S., Fang, X.Q., & Liu, J.X. (2017). Surface energy effect on buckling behavior of the functionally graded nano-shell covered with piezoelectric nano-layers under torque. *International Journal of Mechanical Sciences*, 133, 662–673. https://doi.org/10.1016/j.ijmecsci.2017.09.036.
[14] Ghorbanpour Arani, A., Amir, S., Dashti, P., & Yousefi, M. (2014). Flow-induced vibration of double bonded visco-CNTs under magnetic fields considering surface effect. *Computational Materials Science,* 86, 144–154. https://doi.org/10.1016/j.commatsci.2014.01.047.

[15] Ansari, R., Gholami, R., Norouzzadeh, A., & Darabi, M.A. (2015). Surface Stress Effect on the Vibration and Instability of Nanoscale Pipes Conveying Fluid Based on a Size-Dependent Timoshenko Beam Model. *Acta Mechanica Sinica*, 31, 708-719. https://doi.org/10.1007/s10409-015-0435-4.

[16] Farokhi, H., Païdoussis, M.P., & Misra, A. (2018). Nonlinear behaviour of cantilevered carbon nanotube resonators based on a new nonlinear electrostatic load model. *Journal of Sound and Vibration,* 49, 604-629. https://doi.org/10.1016/j.jsv.2017.09.003.

[17] Pourkiaee, S.M., Khadem, S.E., Shahgholi, M., & Bab, S. (2017). Nonlinear modal interactions and bifurcations of a piezoelectric nanoresonator with three-to-one internal resonances incorporating surface effects and van der Waals dissipation forces. *Nonlinear Dynamocs*, 88, 1785–1816. https://doi.org/10.1007/s11071-017-3345-0.

[18] Sahmani, S., Aghdam, M.M., & Bahrami, M. (2017). Nonlinear buckling and postbuckling behavior of cylindrical shear deformable nanoshells subjected to radial compression including surface free energy effects. *Acta Mechanica Solida Sinica*, 30, 209–22. https://doi.org/10.1016/j.camss.2017.02.002.

[19] Hashemi Kachapi, S.H. (2023). Nonlinear vibration response of piezoelectric nanosensor: influences of surface/interface effects. *Facta Universitatis-Series Mechanical Engineering*, 21(2), 259-272. https://doi.org/10.22190/FUME210612064K.

[20] Hashemi Kachapi, S.H. (2022). Surface/interface approach in pull-in instability and nonlinear vibration analysis of fluid-conveying piezoelectric nanosensor. *Mechanics Based Design of Structures and Machines*, *50*(3), 741–766. https://doi.org/10.1080/15397734.2020.1725566.

[21] Hashemi Kachapi, S.H. (2021). Vibration analysis of multi walled piezoelectric nanoresonator conveying fluid flow: influences of surface/interface energy and walled number effects, Journal of Applied Mathematics and Mechanics (Zeitschrift für Angewandte Mathematik und Mechanik), 101(2), e201900335. https://doi.org/10.1002/zamm.201900335.

[22] Hashemi Kachapi, S.H. (2020). Fluid-conveying piezoelectric nanosensor: Nonclassical effects on vibration-stability analysis. *Structural Engineering and Mechanics, An International Journal*, 76 (5), 619-629. https://doi.org/10.12989/sem.2020.76.5.001.

[23] Ghorbanpour Arani, A., Kolahchi, R., & Hashemian, M. (2014). Nonlocal surface piezoelasticity theory for dynamic stability of double-walled boron nitride nanotube conveying viscose fluid based on different theories. *Proceedings of the Institution of Mechanical Engineers, Part C: Journal of Mechanical Engineering*, 17(228), 3258-3280. https://doi.org/10.1177/0954406214527270.

[24] Wang, L., & Ni, Q. (2009). A reappraisal of the computational modelling of carbon nanotubes conveying viscous fluid. *Mechanics Research Communications*, 7(36), 833–837. https://doi.org/10.1016/j.mechrescom.2009.05.003.

[25] Amabili, M. (2008). Nonlinear Vibrations and Stability of Shells and Plates. New York: Cambridge University Press.